Methods for Multimodal Vibration Suppression and Energy Harvesting Using Piezoelectric Actuators

Justin Wilhelm

Rajesh Rajamani
e-mail: rajamani@me.umn.edu

Department of Mechanical Engineering,
University of Minnesota,
1100 Mechanical Engineering,
111 Church Street South East,
Minneapolis, MN 55455

This paper presents a novel method for suppressing multimodal vibrations in structures by using the controlled harvesting and storage of vibration energy as electrical charge. Unlike a traditional semi-active system in which vibration energy is dissipated using a controlled variable dissipater, the proposed system harvests vibration energy for storage. The stored energy can then be recycled enabling the system to achieve a vibration reduction performance superior to that of a traditional semi-active system and approaching that of a fully active system. In the proposed method, an array of one or more precharged capacitors is employed to provide a selection of various voltages, which may be selected to approximate a desired control signal defined by an LQR multimodal vibration controller. The capacitors can apply a control voltage to the piezoelectric actuators and can also collect current generated by the actuators as the structure strains in vibration. Both a single capacitor system and a multi-capacitor system are considered and applied to a cantilevered beam. The response to impulse disturbances and random force disturbances are studied. The results are compared to a previously proposed energy harvesting based semi-active method. Advantages in both vibration suppression and energy harvesting performance over the previously proposed method are demonstrated. The multicapacitor method is found to be most effective due to its ability to apply sufficiently large control voltages while moderating large step inputs therefore reducing the excitation of higher frequency uncontrolled modes, which otherwise parasitically dissipate energy in the circuit resistance. [DOI: 10.1115/1.2980378]

1 Introduction

Piezoelectric elements are attractive candidates for use as both vibration suppression actuators and sensors because of the convenient electrical-mechanical coupling they provide. Over the past two decades, considerable research has been conducted to explore the integration of piezoelectric elements into active and passive vibration control. Passive techniques have been popular because of their inherent stability and, in most cases, lack of reliance on an external power source. Passive techniques employ shunts of impedances designed to effectively dissipate electrical energy transduced from mechanical vibration energy. Some of the more successful systems place a resistor and an inductor in the shunt networks to react with the inherent capacitance of the piezoelectric elements to form resonant circuits. Such systems have been shown to reduce resonant vibration amplitudes by 15–20 dB [1]. The necessity for very large inductors (hundreds of Henrys in some cases) to implement these systems poses a significant disadvantage in many situations. These inductors may be implemented using active electronic elements; however, this sacrifices some of the appeal in simplicity and power independence of these systems. Furthermore, small changes in the mechanical system dynamics can greatly reduce the effectiveness of such resonant circuits [2].

Energy harvesting semi-active methods offer promise in their more general ability to suppress vibrations while requiring very little if any external power. More recently, Makihara, et al. [3,4] have proposed a method similar to a method proposed by Corr and Clark [5] that combines a resistor-inductor (RL) circuit with synchronized switching strategies to suppress vibrations using energy harvested from the vibration itself. Although, these techniques exhibit a higher complexity than the strictly passive networks, they offer a similar level of vibration suppression using much smaller inductors and are not as sensitive to subtle changes in or to inaccurate estimates of the mechanical resonant properties. Makihara et al. [3] take an optimal control approach to determine appropriate control voltages and then actuate a switch in the circuit to send all of the acquired charge in the system to one electrode or to the other corresponding to the polarity of the optimal control. While this has been shown to work reasonably well with single mode mechanical systems, the results of this method are not as desirable in multimode systems [3,4]. Furthermore, since the energy for control effort originates from vibration energy, when transient disturbances are encountered, significant control gains are not available until well into the transient interval, and the suppression of the disturbance is delayed. At the conclusion of each transient event, high frequency oscillations dispose of the acquired energy into the circuit resistance leaving no residual energy to suppress future transient disturbances or to provide power for control and switching circuitry. Apart from the limitations in the method's vibration suppression, it does not meet the criteria of a more strict definition of "energy harvesting" adopted by the author that requires the energy to be absorbed and stored in a manner such that it may be used for ancillary power requirements in addition to continuing vibration suppression.

In the field of energy harvesting, a number of different researchers have worked on the development of algorithms and power electronics to maximize the energy harvested from a given level of vibrations [6–9]. The simplest energy harvesting algorithm uses a voltage rectifier, a storage capacitor to store charge, and a fixed threshold algorithm that switches the power stored in the capacitor to power a load at predetermined levels of voltage.

Contributed by the Technical Committee on Vibration and Sound of ASME for publication in the JOURNAL OF VIBRATION AND ACOUSTICS. Manuscript received July 19, 2007; final manuscript received July 18, 2008; published online December 29, 2008. Assoc. Editor: William W. Clark.

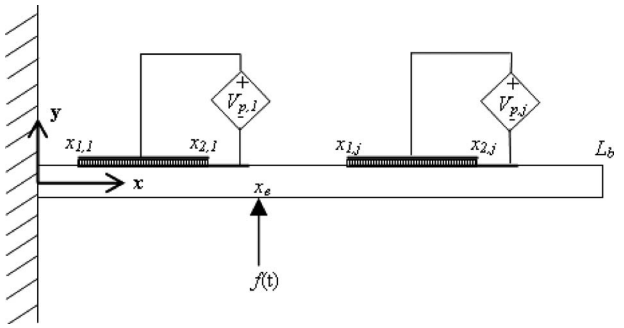

Fig. 1 Schematic of the cantilevered beam system

These pre-determined threshold values must change with the amplitude and frequency of vibrations in order to maximize the harvested energy. A number of different control algorithms that provide significantly improved energy harvesting compared to the constant threshold values include (a) impedance adaptation algorithms in which a gradient based adaptive algorithm is used to continuously change the switching voltage thresholds [6,7] and synchronous charge extraction algorithms in which the extraction of electrical charge is synchronized with mechanical vibrations [9].

The method proposed in this paper seeks to combine the two objectives of vibration reduction and energy harvesting. The proposed method seeks to implement optimal vibration control using harvested energy that will be continually available for vibration suppression and control circuitry power. This method is unique from previously proposed methods in that control voltages are provided by external capacitors that also absorb the electrical energy they are resisting and even more so in that an array of capacitors are used to provide a range of voltages to approximate the optimal control voltage with some level of fidelity.

The power requirement for processing the control algorithms and switching are considered to be outside the scope of this paper and are not considered herein. Ideally, the scale of the mechanical system and its vibrations, as well as the power requirements of the electronic circuitry, would allow the proposed method to be at least partially self-powering. Before this method is described in detail, the subject plant is established and described in Sec. 2.

2 System Model

The system of interest, depicted in Fig. 1, is a cantilevered beam with relatively thin patches of piezoelectric material adhered to one or more regions of one surface.

As demonstrated clearly by Makihara et al. [3], a dynamic model for a cantilevered beam with attached piezoelectric actuators may be derived through the use of Hamilton's principle and the Euler–Bernouli model for the mechanics of a beam in flexure. The kinetic energy in the beam and the attached piezoelectric actuators is expressed in Eqs. (1) and (2), respectively.

$$T_b = \int_0^{L_b} \tfrac{1}{2}\rho_b A_b \left(\frac{\partial w_y}{\partial t}\right)^2 dx \tag{1}$$

$$T_{pj} = \int_0^{L_b} \tfrac{1}{2}\rho_{pj} A_{pj} \left(\frac{\partial w_y}{\partial t}\right)^2 g_j(x)\,dx \tag{2}$$

where

$$g_j(x) \equiv H(x - x_{2j}) - H(x - x_{1j})$$

and $H(x)$ is the Heaviside function.

The potential energy in the beam and the attached actuators is expressed in Eqs. (3) and (4).

$$U_b = \int_0^{L_b} \frac{1}{2} c_b I_b \left(\frac{\partial^2 w_y}{\partial x^2}\right)^2 dx \tag{3}$$

$$U_{pj} = \int_{V_{pj}} (\sigma_x \varepsilon_x + E_y D_y)\,dV \tag{4}$$

The virtual work on the system, expressed in Eq. (5), comes from work done by external forces on the beam, as well as the electrical work performed on actuators.

$$\delta W = \int_0^{L_b} f(x,t)\,\delta w_y dx + \sum_{j=1}^{n_p} V_j \times \int_{A_{pj}} \delta D_{yj} g_j(x)\,dA \tag{5}$$

The lateral displacement of the beam at each point along its length can be approximated by a finite series of assumed mode functions.

$$w_y(x,t) = \sum_{k=1}^{n} p_k(t)\,\psi_k(x) \tag{6}$$

In this case, the assumed mode functions are taken as the standard eigenfunctions for a cantilevered beam, which may be found in many vibration texts [10]. These functions are orthogonal over the full length of the beam, but not over the intervals covered by the actuators.

Applying Eq. (6), as well as the one-dimensional piezoelectric constitutive equations

$$E_y = -b_p \varepsilon_x + \frac{D_y}{e_p^S} \tag{7}$$

$$\sigma_x = c_p \varepsilon_x - b_p D_y \tag{8}$$

Hamilton's principle yields the following dynamic equations:

$$(\mathbf{M}_b + \mathbf{M}_p)\ddot{\boldsymbol{p}} + (\mathbf{K}_b + \mathbf{K}_p)\boldsymbol{p} = \mathbf{B}_a \boldsymbol{Q} + \mathbf{B}_e \boldsymbol{f} \tag{9}$$

$$\boldsymbol{V}_p = -\mathbf{B}_a^T \boldsymbol{p} + \mathbf{C}_a^{-1} \boldsymbol{Q} \tag{10}$$

$$\mathbf{M}_b \equiv \text{diagonal}\left[\rho_b A_b \int_0^{L_b} \psi_k \psi_k dx\right]$$

$$\mathbf{K}_b \equiv \text{diagonal}\left[c_b I_b \int_0^{L_b} \frac{\partial^2 \psi_k}{\partial x^2}\frac{\partial^2 \psi_k}{\partial x^2} dx\right]$$

$$\mathbf{C}_a \equiv \text{diagonal}\left[\frac{e_p^S \eta_b^2 (x_{2j} - x_{1j})}{A_{pj}}\right]$$

$$\mathbf{M}_p \equiv \sum_{j=1}^{n_p} \rho_{pj} A_{pj} \int_{x_{1j}}^{x_{2j}} \psi_k \psi_k dx$$

$$\mathbf{K}_p \equiv \sum_{j=1}^{n_p} c_{pj} I_{pj} \int_{x_{1j}}^{x_{2j}} \frac{\partial^2 \psi_k}{\partial x^2}\frac{\partial^2 \psi_k}{\partial x^2} dx$$

$$\mathbf{B}_a \equiv -\frac{b_{pj} J_{pj}}{\eta_b (x_{2j} - x_{1j})} \int_{x_{1j}}^{x_{2j}} \frac{\partial^2 \psi_k}{\partial x^2} dx$$

$$\mathbf{B}_e \equiv \left.\psi_k(x)\right|_{x=x_e}$$

External forces are assumed to be applied at a single point, x_e. That is

$$f(x,t) = \delta(x - x_e) f_e(t).$$

Equations (9) and (10) are rearranged to treat actuator voltages as inputs.

$$\ddot{\mathbf{p}} + \mathbf{\Xi}\dot{\mathbf{p}} + \mathbf{\Omega}\mathbf{p} = \mathbf{B}_1 V_p + \mathbf{B}_2 \mathbf{f} \tag{11}$$

$$\mathbf{B}_1 \equiv (\mathbf{M}_b + \mathbf{M}_p)^{-1}\mathbf{B}_a\mathbf{C}_a$$

$$\mathbf{B}_2 \equiv (\mathbf{M}_b + \mathbf{M}_p)^{-1}\mathbf{B}_e$$

$$\mathbf{\Omega} \equiv (\mathbf{M}_b + \mathbf{M}_p)^{-1}(\mathbf{K}_b + \mathbf{K}_p - \mathbf{B}_a\mathbf{C}_a\mathbf{B}_a^T)$$

$$\mathbf{\Xi} \equiv \text{diagonal}[\zeta\omega_k]$$

In modal analysis, the damping ratio is not typically determined analytically, but rather determined empirically. It this paper, it is assumed to be 0.01.

As mentioned above, the assumed mode functions are not orthogonal over the actuator intervals. As a result $\mathbf{M}_p$ and $\mathbf{K}_p$ are not diagonal and the modes of the system described in Eq. (11) are coupled. To diagonalize this system and decouple the modes, a second general eigenvector problem is solved.

$$(\mathbf{K}_b + \mathbf{K}_p - \mathbf{B}_a\mathbf{C}_a\mathbf{B}_a^T)\mathbf{\Phi} - (\mathbf{M}_b + \mathbf{M}_p)\mathbf{\Phi}\mathbf{\Lambda} = \mathbf{0} \tag{12}$$

These new eigenvectors are used to define a new set of modal eigenfunctions and to transform the matrices defined above.

$$[\Psi_1 \quad \Psi_2 \quad \cdots \quad \Psi \quad N] \equiv [\psi_1 \quad \psi_2 \quad \cdots \quad \psi_N]\mathbf{\Phi} \tag{13}$$

$$w_y(x,t) \equiv \sum_{k=1}^{N} \xi_k(t)\Psi_k(x) \tag{14}$$

$$\bar{\mathbf{K}}_b \equiv \mathbf{\Phi}^T\mathbf{K}_b\mathbf{\Phi}$$

$$\bar{\mathbf{K}}_p \equiv \mathbf{\Phi}^T\mathbf{K}_p\mathbf{\Phi}$$

$$\bar{\mathbf{M}}_b \equiv \mathbf{\Phi}^T\mathbf{M}_b\mathbf{\Phi}$$

$$\bar{\mathbf{M}}_p \equiv \mathbf{\Phi}^T\mathbf{M}_p\mathbf{\Phi}$$

$$\bar{\mathbf{B}}_a \equiv \mathbf{\Phi}^T\mathbf{B}_a$$

$$\bar{\mathbf{B}}_e \equiv \mathbf{\Phi}^T\mathbf{B}_e$$

$$\bar{\mathbf{\Omega}} \equiv \mathbf{\Phi}^T\mathbf{\Omega}\mathbf{\Phi} = \mathbf{\Lambda} = \text{diagonal}[\omega_k^2]$$

Defining the state as

$$z \equiv [\vec{\xi}^T \quad \dot{\vec{\xi}}^T]^T$$

provides the following state space realization in which each mode is decoupled except for the overlapping influence of the input matrix.

$$\dot{z} = \mathbf{A}\mathbf{z} + \mathbf{B}_3\mathbf{V}_p + \mathbf{D}\mathbf{f} \tag{15}$$

$$\mathbf{A} \equiv \begin{bmatrix} \mathbf{0} & \mathbf{I} \\ -\bar{\mathbf{\Omega}} & -\mathbf{\Xi} \end{bmatrix}$$

$$\mathbf{B}_3 \equiv \begin{bmatrix} \mathbf{0} \\ \bar{\mathbf{B}}_1 \end{bmatrix}$$

$$\mathbf{D} \equiv \begin{bmatrix} \mathbf{0} \\ \bar{\mathbf{B}}_2 \end{bmatrix}$$

Since the modes are decoupled and each mode is asymptotically stable, the infinite dimensional system may be truncated to a reasonable number of modes with minimal detriment. In this paper the first ten modes will be modeled, and the first three will be controlled.

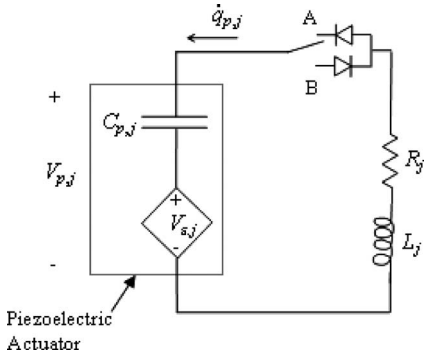

Fig. 2 Diagram for the RL switching circuit

3 Control System

In this paper, vibration suppression is pursued in the context of LQR optimal control [11,12]. While less structured modal velocity feedback control is conceivable, LQR simplifies the task of determining appropriate gains to accomplish the vibration suppression and energy harvesting objectives in the context of complex and interconnected input-output relationships. Observability of the system described above can be guaranteed by placing sensors such that their domain of sensitivity to each mode is not dominated by modal node phenomena. Also, Kalman filters and other state estimators are routinely employed in estimating modal states for the control of flexible structures; therefore, in the interest of simplicity, it is assumed that a suitable estimate of the full state is available for feedback. The details of the state estimation are not central to the investigation in this paper and are therefore disregarded.

The goal for this control task is to minimize the following cost function:

$$J \equiv \int_0^\infty (\mathbf{z}\mathbf{W}_1\mathbf{z} + \mathbf{V}_c\mathbf{W}_2\mathbf{V}_c + 2\mathbf{z}\mathbf{W}_3\mathbf{V}_c)dt \tag{16}$$

Weighting matrices, $\mathbf{W}_1$, $\mathbf{W}_2$, and $\mathbf{W}_3$, are chosen to tune the vibration suppression performance and balance it with the energy harvesting capacity while keeping the underlying quadratic form matrix positive definite.

The optimal control voltages, $\boldsymbol{V}_c$, are then defined as,

$$\mathbf{V}_c \equiv \mathbf{F}\mathbf{z} = \mathbf{W}_2^{-1}(\mathbf{B}_3^T\mathbf{P} + \mathbf{W}_3^T)\mathbf{z} \tag{17}$$

where $\mathbf{F}$ is the LQR feedback gain matrix and $\mathbf{P}$ is the solution to the applicable Riccati equation.

Three different means of delivering an approximation of the control voltages from Eq. (17) are investigated in this paper.

3.1 RL Switching. The first method studied is the one proposed by Makihara et al. [3,4]. A schematic of this system is shown in Fig. 2.

The piezoelectric actuators are modeled as a voltage supply representing the potential generated as the polarized crystal structure strains, and a capacitor in series, which reflects the potential across the actuator due to built up charge, as well as the limit to the charge flow that the actuator may produce. Kirchoff's voltage law gives the differential equation for the charge on the piezoelectric actuator when current is free to flow.

$$V_{\varepsilon,j} + \frac{q_{p,j}}{C_{p,j}} + \dot{q}_{p,j}R_j + \ddot{q}_{p,j}L_j = 0 \tag{18}$$

$$\vec{V}_\varepsilon \equiv \mathbf{B}_a\vec{z}$$

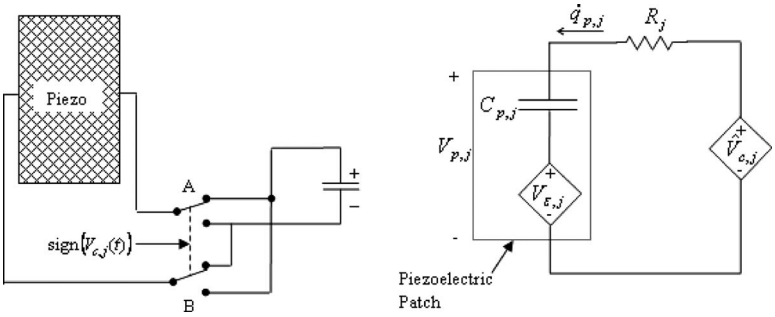

Fig. 3 Schematic and circuit diagram of the single switched capacitor method

In fact, the current is not allowed to flow freely, the switch (A/B) is used to control the current to apply and maintain a charge on one electrode or the other according to the following switching law:

$$\text{If } V_{c,j} > 0 \quad \text{then turn the } j\text{th switch to } A$$
$$\text{If } V_{c,j} < 0 \quad \text{then turn } j\text{th switch to } B \tag{19}$$

At $t=0$, there is no charge on the actuator electrodes. As the beam displacement strains the actuator, it generates a positive/negative voltage that motivates a negative/positive current, which builds a negative/positive charge on the actuator until the charge induced potential equalizes the rest of the loop voltages, which occurs when the beam deflection is at a maximum magnitude. The diode prevents a reverse in current. The charge on the actuator remains constant until $t=t_k$ when the switch is actuated, which will typically occur just as the beam deflection velocity begins to reverse, and the current is free to flow in the opposite direction. The underdamped second order behavior of the RL circuit allows the majority of the charge energy collected during the first actuator displacement to be transferred to the opposite electrode with a time constant much shorter than the vibration period. During the second displacement, the strain in the actuator adds potential on top of the potential due to the existing charge such that when the switch is actuated again, an even larger amount of energy is transferred to the opposite electrode. The cycle continues converting more and more mechanical energy into charge energy on the piezoelectric actuator. The charge on and the potential across the actuator electrodes are governed by the following laws:

$$q_{p,j,k} = \begin{cases} \dfrac{1}{L_j}\displaystyle\int_{t_k}^{t_k+\Delta t}\left[-\dot{q}_{p,j}R_j - \int_{t_k}^{t_k+\Delta t}\left(V_{\varepsilon,j} + \frac{q_{p,j,k}}{C_{p,j}}\right)dt\right]dt + q_{p,j,k-1} & A \text{ and} \left(V_{L,j} > \dfrac{q_{p,j}}{C_{p,j}}\right) \\ q_{p,j,k} & A \text{ and} \left(V_{L,j} \leqslant \dfrac{q_{p,j}}{C_{p,j}}\right) \\ \dfrac{1}{L_j}\displaystyle\int_{t_k}^{t_k+\Delta t}\left[-\dot{q}_{p,j}R_j - \int_{t_k}^{t_k+\Delta t}\left(V_{\varepsilon,j} + \frac{q_{p,j,k}}{C_{p,j}}\right)dt\right]dt + q_{p,j,k-1} & B \text{ and} \left(V_{L,j} < \dfrac{q_{p,j}}{C_{p,j}}\right) \\ q_{p,j,k} & B \text{ and} \left(V_{L,j} \geqslant \dfrac{q_{p,j}}{C_{p,j}}\right) \end{cases} \tag{20}$$

where a loop voltage is defined as

$$V_{L,j} \equiv -V_{\varepsilon,j} - \ddot{q}_{p,j}L_j - \dot{q}_{p,j}R_j$$
$$V_{p,j,k} \equiv V_{\varepsilon,j} + \frac{q_{p,j,k}}{C_{p,j}} \tag{21}$$

Some drawbacks of this method were briefly discussed in the introduction. Mainly, the method's need to pass all of the stored energy through a resistive circuit each time the input polarity is reversed limits the amount of energy the system can harvest from the mechanical vibration, and the method's inability to permanently store energy limits its effectiveness in suppressing transient disturbances. These limitations motivate the first proposed alternative method.

3.2 Single Switched Capacitor. The single switched capacitor (SSC) method works in a similar manner to the RL switiching (RLS) method above except for a few differences in implementation. First, instead of storing power in the very small capacitance of the actuator, energy is stored in a large external capacitor. Second, instead of passing the stored charge through an RL circuit to reverse the potential across the actuator electrodes, the leads to the capacitor are swapped by switches so that the charge potential on the actuator is immediately reversed with minimal charge flow avoiding wasted energy in the circuit resistance. A schematic and circuit diagram of this system is shown in Fig. 3. The voltage source, $\hat{V}_c$, represents an approximation, a very rough approximation in this case, of the optimal input voltage. This approximation is a constant voltage with the same polarity as the prescribed optimal input voltage. The switching law for this law is identical as that for the RLS method in Eq. (19) except that a small threshold (1 V) is set such that when vibrations are sufficiently small, the controller goes dormant to conserve energy and to allow the structure to settle to equilibrium leading to the following switching law:

$$\text{If } V_{c,j} > V_t \quad \text{then turn } j\text{th switch to } A$$

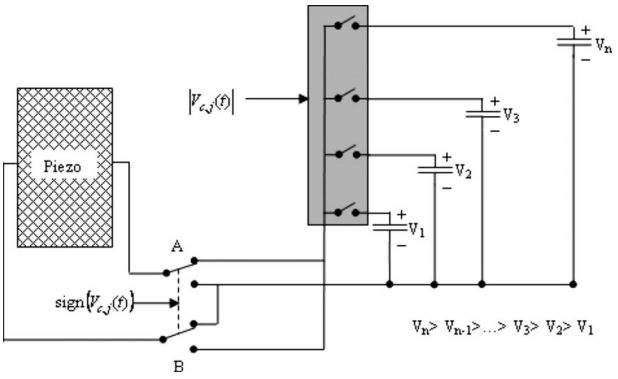

Fig. 4 Schematic of the multiple switched capacitor method

$$\text{If } V_{c,j} < -V_t \quad \text{then turn } j\text{th switch to } B \tag{22}$$

$$\text{If } -V_t < V_{c,j} < V_t \quad \text{then turn } j\text{th switch to open}$$

Kirchoff's voltage law gives the following differential equation for the charge on the piezoelectric actuator:

$$V_{\varepsilon,j} + \frac{q_{p,j}}{C_{p,j}} + \dot{q}_{p,j}R_j - \hat{V}_{c,j} = 0 \tag{23}$$

$$\dot{q}_{p,j} = \frac{1}{R_j}\left(-\frac{q_{p,j}}{C_{p,j}} - V_{\varepsilon,j} + \hat{V}_{c,j}\right) \tag{24}$$

The very small capacitance of the actuator gives an extremely fast time constant such that the charge will reach steady state in a time interval much less than the period of even the fastest modeled vibration mode. For this reason, the charge is assumed to be at steady state indefinitely such that the current only results from changes in the steady state conditions.

$$\dot{q}_{p,j} \approx C_{p,j}(\dot{\hat{V}}_{c,j} - \dot{V}_{\varepsilon,j}) = i_{p,j} \tag{25}$$

The voltage applied to the piezoelectric actuator is expressed as

$$V_{p,j} \equiv \hat{V}_{c,j} - i_{p,j}R_j = \hat{V}_{c,j} - R_jC_{p,j}(\dot{\hat{V}}_{c,j} - \dot{V}_{\varepsilon,j}) \tag{26}$$

and the current flowing into the main capacitor is expressed as

$$i_{c,j} \equiv -i_{p,j} = -C_{p,j}(\dot{\hat{V}}_{c,j} - \dot{V}_{\varepsilon,j}) \tag{27}$$

It follows that the energy stored in the main capacitor is calculated as

$$U_{c,j} \equiv \frac{1}{2C_{c,j}}\left\{\int_{t_0}^{t}[-C_{p,j}(\dot{\hat{V}}_{c,j}(\tau) - \dot{V}_{\varepsilon,j}(\tau))]d\tau\right\}^2 + U_{c,j}(t_0) \tag{28}$$

Values of $C_{c,j}$ are preferably large such that the nominal voltage changes little as electrical energy is absorbed. Nonetheless, the practical implementation of this method would require a separate energy management system that would re-allocate the charge in the capacitor to a secondary storage device or consume the energy in some other manner to maintain the nominal voltage.

3.3 Multiple Switched Capacitors. The third method to be investigated utilizes multiple capacitors precharged to different voltages such that the optimal control voltage may be more closely approximated. A schematic of this system is shown in Fig. 4. The circuit diagram and electrical differential equations are the same as for the previous method. The switching for this method follows Eq. (22); however, beyond switching for the correct polarity, switching also occurs to connect the capacitor whose potential is the closest to the optimal voltage without being larger as portrayed in Fig. 4.

An optimal choice of the number of capacitors to use and to what voltage they should be charged may exist; however, this optimum will likely be based on a particular application and is beyond the scope of this paper. The number of capacitors in this case has been set to seven. Counting a zero level, this gives eight different levels: a convenient number for digital implementation. In order to provide a few smaller closer voltage levels that can more effectively deal with small vibrations while maintaining much larger voltage levels to handle severe vibrations or disturbances, an exponential progression of potentials are selected for the seven capacitors. Small deviations from a strictly exponential progression have been made to tailor the selection of potentials to more closely match commonly required control voltages. The potentials selected for the multiple switched capacitor (MSC) method simulated in this paper are shown in Fig. 5.

As with the SSC method, values of $C_{c,j}$ are preferably large such that the nominal voltage changes little as the electrical energy is absorbed; however, a separate energy management system would be required to maintain the nominal capacitor voltages. It should also be noted that the circuit models above are based on ideal circuits where, other than in discrete circuit components, the circuit capacitance and inductance are assumed to be zero and high frequency electrical oscillations and the radiation of electromagnetic energy, likely to result from the stepped voltage changes in the methods discussed above, are assumed to be relatively insignificant and are neglected in the simulations to follow.

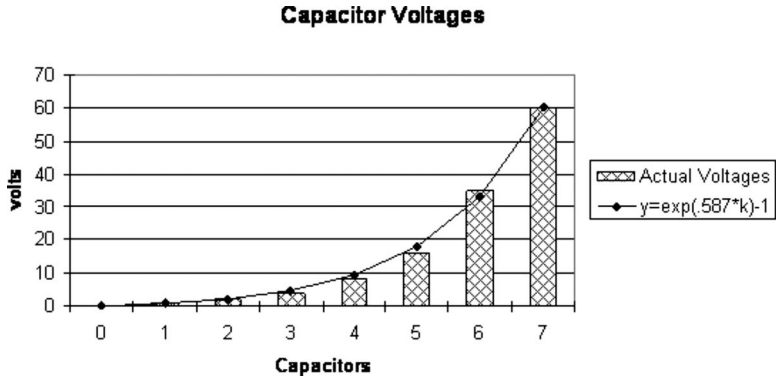

Fig. 5 Preset voltages of capacitors for the multiple switched capacitor method

Table 1 System parameters

n_p	2	x_{11}	0.0×10^{-1} m
η_p	2.0×10^{-1} m	x_{12}	2.0×10^{-1} m
h_p	2.52×10^{-3} m	x_{21}	4.0×10^{-1} m
ρ_p	7.5×10^{3} kg/m^3	x_{22}	6.0×10^{-1} m
c_b	7.1×10^{10} N/m^2	L_b	1.0×10^{0} m
b_p	8.9×10^{8} N/C	η_b	2.0×10^{-1} m
e_p^S	1.4×10^{-1} m	h_b	2.5×10^{-3} m
		ρ_b	2.7×10^{3} kg/m^3
		c_b	7.1×10^{10} N/m^2

4 Simulation Studies

The cantilevered beam system described above was simulated using the parameters in Table 1. These were chosen to be the same as those used by Makihara et al. [3] for the purpose of direct comparison to the results given in that paper.

4.1 Control System Preliminaries. The first three assumed mode shapes corresponding to a cantilevered beam [10] without attached piezoelectric actuators are shown in Fig. 6. The strain at the surface of the beam along its length is related directly to the second derivative of lateral displacement of the beam and thus directly related to the second derivative of the mode functions, which are shown in Fig. 7. Examining this graph brings understanding of the rationale for the choice of actuator placement. In the first region, 0–0.2 m, the second derivatives of all three modes are large providing a strong actuator to mode coupling. In the second region, 0.4–0.6 m, the net strain of the second mode has large and negative strain, and the third mode is nearly zero. An actuator placed in this location has some independence from the first region allowing the different modes to be addressed simultaneously with smaller control effort.

Figure 8 shows the actual mode shapes, from Eq. (13), with the piezoelectric actuators attached. Stiffening of the beam in actuator regions is evident. Based on the parameters in Table 1, the natural frequencies corresponding to the first three modes are 3.4 Hz, 19.4 Hz, and 49.4 Hz.

A set of LQR weight matrices were determined by Makihara et al. [3] to be approximately optimal for the RLS. Since the actual magnitude of the input cannot be controlled in the RLS method, the relative magnitude relationships between the matrix components are relevant while the absolute magnitude of the set of components is not. These weighting matrices are not appropriate for the other two methods for similar, but slightly different reasons.

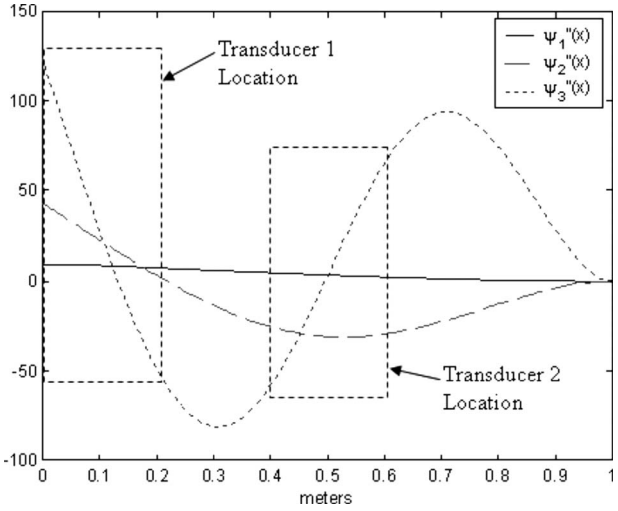

Fig. 7 Mode function second derivatives

First, in the SSC method, the magnitude of the optimal control is important because a threshold must be surpassed for the switch to close according to Eq. (22). Second, in the MSC method, the magnitude of the optimal voltage is especially important since it will actually be approximated through the selection among an array of capacitors at different voltages. The following set of weighting matrices were found to give reasonably good and balanced vibration suppression and energy harvesting performance.

$$W_1 = \text{diagonal}\left[4\times10^{10}, 1, 1, \frac{4\times10^{10}}{\omega_1^2}, \frac{2\times10^{10}}{\omega_2^2}, \frac{1\times10^{10}}{\omega_3^2}\right]$$

$$W_2 = \text{diagonal}[2,1]$$

$$W_3 = 10^2 \times \begin{bmatrix} 0 & 0 & 0 & 0 & 10 & 0 \\ 0 & 0 & 0 & 0 & 0 & 6 \end{bmatrix}^T$$

It is evident that the first matrix is heavily weighted toward velocity damping. As a result, the majority of the vibration suppression is achieved through damping. The damping action tends to apply forces against velocity and, in this case, voltage against current, which is beneficial for energy harvesting objectives.

The third matrix applies to the cross terms of the underlying quadratic form to penalize situations where the actuator current

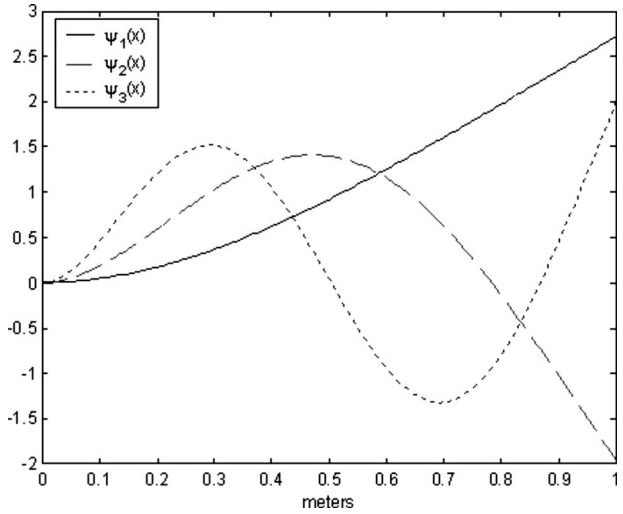

Fig. 6 Mode functions of the cantilevered beam

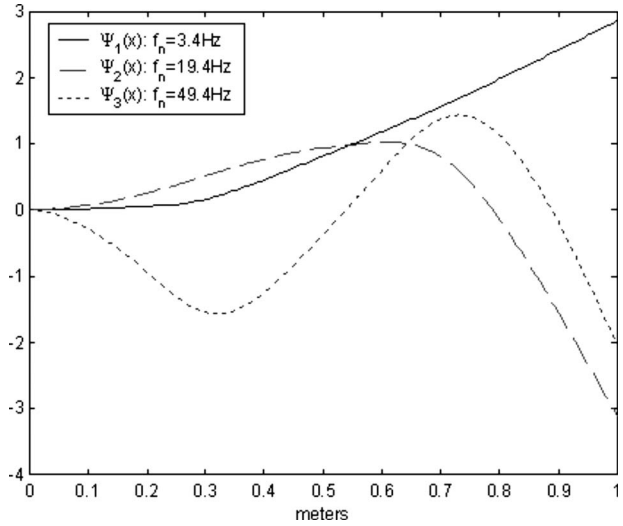

Fig. 8 Corrected mode functions for the diagonalized system

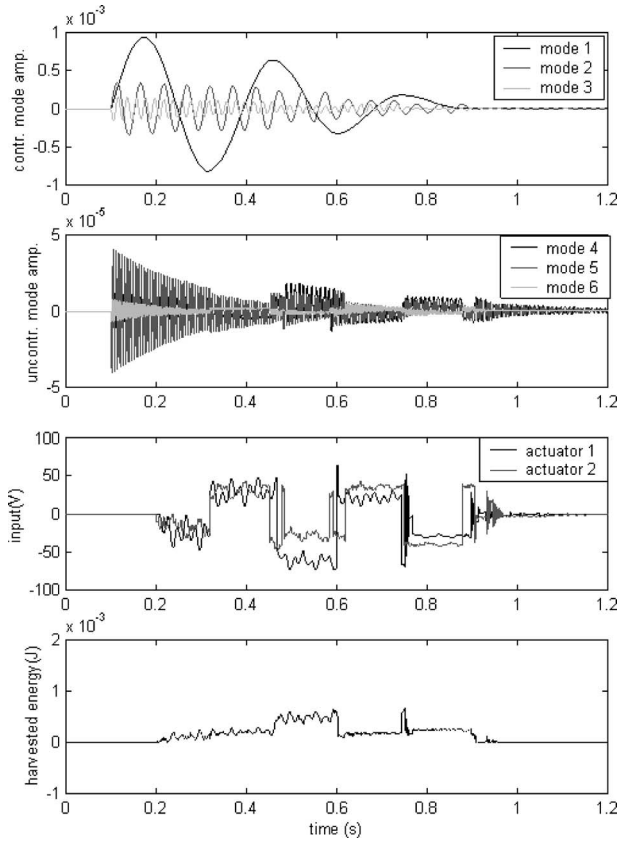

Fig. 9 Impulse test results for the RL switching

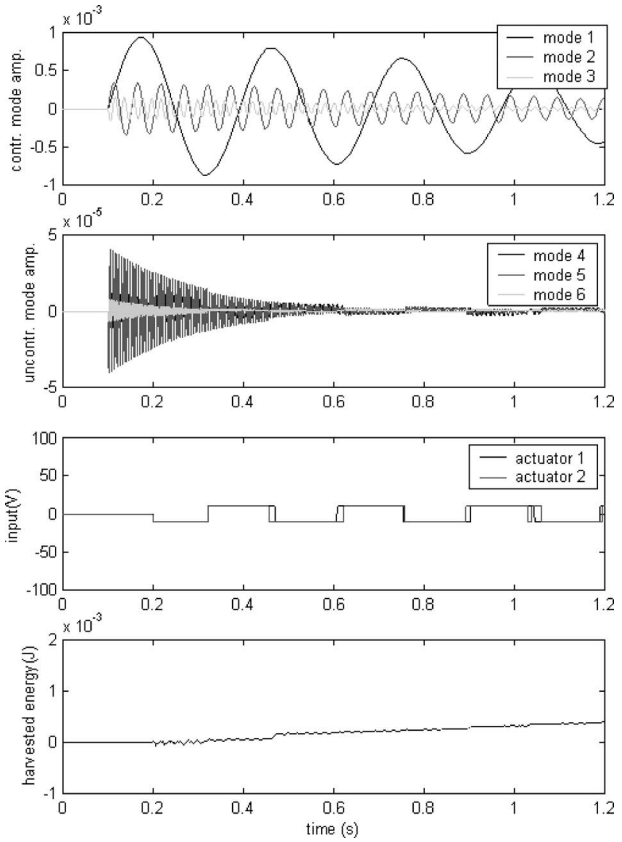

Fig. 10 Impulse test results for the single switched capacitor

flows with the voltage drawing power out of the capacitors. Positive velocities of the second and third modes induce negative actuator strain rates promoting charge flow into the second and first actuators, respectively. To avoid situations where voltage and current align to give up energy back to the beam, a weight is placed on the cross products of the appropriate input voltages and modal velocities. Since these components are off the diagonal, their values are constrained such that the underlying quadratic form matrix remains positive definite.

4.2 Impulse Tests. MATLAB SIMULINK was used to simulate the application of each of the three methods to the cantilevered beam system. The first performance test conducted for the vibration suppression methods was an impulse test. The system starts at rest. At $t=0.1$ s, an external force in the form of an impulse is applied to the system at $x=x_e=0.4$ m. At $t=t_s=0.2$ s, the vibration control methods were activated. Makihara et al. [4] determined a circuit resistance of 0.5 Ω gives a nearly optimal performance for a given inductance of 1.5 mH. These same values are used for the RLS simulations in this paper. For the single capacitor switching method, the capacitor voltage was loosely optimized for balanced vibration suppression and energy harvesting at 10 V. This will be discussed further in a subsequent section. The methods are rated according to two primary metrics. The first is energy harvesting efficiency, which is defined as

$$\text{eff} = \left(\frac{\sum_{j=1}^{n_p} (U_{c,j}(t_f) - U_{c,j}(t_s))}{T_b(t_s) + U_b(t_s) + \sum_{j=1}^{n_p} (T_{p,j}(t_s) + U_{p,j}(t_s))} \right) \times 100\% \tag{29}$$

The second is a metric of vibration magnitude over time used by Makihara et al. [3].

$$I_{\text{rms}} = \int_{t_s}^{t_f} \delta_{\text{rms}}(t)\mathrm{d}t \tag{30}$$

$$\delta_{\text{rms}}(t) = \sqrt{\frac{1}{L_b}\int_0^{L_b} w_y^2(x,t)\mathrm{d}x} \tag{31}$$

The results of the impulse test for the three methods are shown in Figs. 9–11. The first plot in each figure shows the modal amplitudes for the three controlled modes. Modal amplitudes for the next three uncontrolled modes are shown in the second plot. Amplitudes for the remaining modes are insignificant in comparison to the first six modes and thus are not shown. The third plot shows the input voltages applied to each actuator, and the fourth plot shows the amount of electrical energy stored in the actuators in the case of the RLS method or the external capacitors for the SSC and MSC methods.

The RLS method was quite successful in quickly suppressing the impulse excited vibrations. While the RLS method is quite successful at suppressing the vibration, it cannot store energy unless it is actively actuating. As the transient vibration dies out, all of the energy it has harvested is dumped into the circuit resistance and mechanical damping through high frequency switching.

The SSC method offered a much less significant effect on the vibrations; however, in the last plot of Fig. 10 it is evident that the SSC method steadily collects energy from the vibrations as charge generated by the actuators flows against the potential of the capacitors. Detrimental effects of control voltage clipping on harvesting efficiency are also evident. In order to harvest energy efficiently, the voltage on the capacitor in the SSC method must be limited otherwise the responses of higher modes to the large stepped inputs cause high frequency currents in the control circuits, which dissipate a large amount of energy to the circuit resistance. At the same time, reducing the voltage also compromises

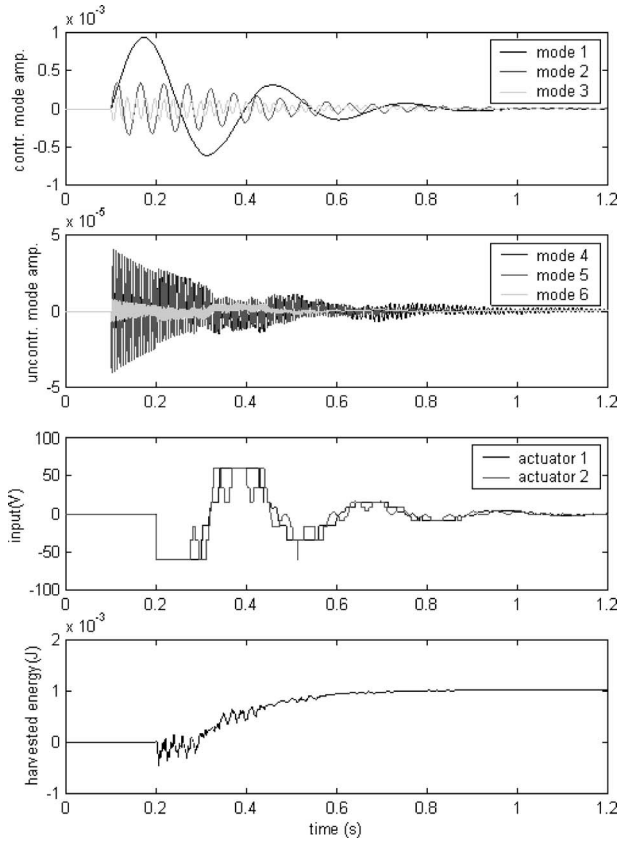

Fig. 11 Impulse test results for the multiple switched capacitors method

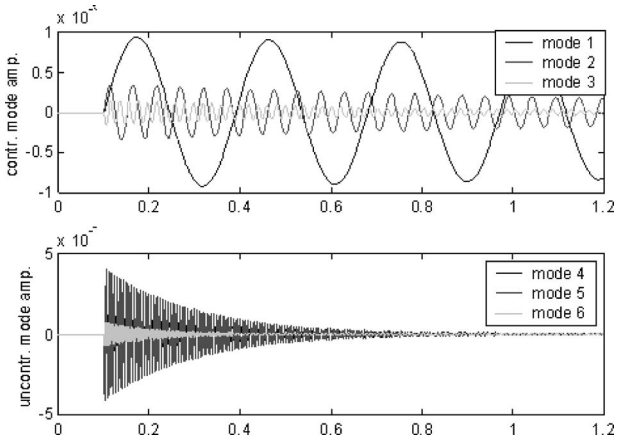

Fig. 12 Impulse response with no vibration suppression applied

the vibration suppression capacity. The results shown here represent a balance allowing reasonable energy harvesting efficiency and vibration suppression not only for the impulse test, but for the random excitation test to be discussed next. If a particular application requires better performance in one aspect or the other, a more optimal balance could be attained.

The MSC method exhibits exceptional performance in both energy harvesting efficiency, as well as vibration suppression. As seen in the harvested energy plot, the MSC method rapidly collects electrical energy while vibration energy is abundant and then plateaus as the mechanical energy source is depleted. It should be noted that the performance of the MSC method requires that the capacitor voltages are chosen to appropriately match the system and the set of expected disturbances. If the disturbances are large enough to require inputs that saturate the range of the set of capacitors, problems similar to those described for the SSC method will arise, and the energy harvesting efficiency, not to mention the vibration suppression capacity, will suffer.

Figure 12 presents the impulse response of the system without any external vibration suppression applied as a relative reference to the results above. Table 2 below contains the energy harvesting and vibration suppression metrics for each method.

4.3 Random Excitation Tests. The second test subjected the beam and each of the methods to each of five different random external force time sequences. The five time histories were generated using an inverse fast Fourier transform (FFT) of a uniform power spectral density spanning from 2 Hz to 50 Hz, covering each of the three controlled modes and random phase alignments. Limiting the bandwidth of the random input to the first three modes is considered legitimate since prudent practice would seek to control all modes that are significantly excited by typical persistent disturbances. Simulations of the random excitation tests began with 12 s of excitation to allow the vibration in the beam to stabilize. At $t=t_s=12$, the vibration suppression methods were activated, and the same performance metrics as above were used with only a slightly different definition for the efficiency metric to account for work performed on the system by the external force.

$$\text{eff} = \left(\frac{\Sigma_{j=1}^{n_p} (U_{c,j}(t_f) - U_{c,j}(t_s))}{T_b(t_s) + U_b(t_s) + \sum_{j=1}^{n_p} (T_{p,j}(t_s) + U_{p,j}(t_s)) + \int_{t_s}^{t_f} f(t) \cdot \frac{\partial w_y(x_e,t)}{\partial t} \mathrm{d}t} \right) \times 100\% \tag{32}$$

The results of the random excitation test with random force sequence 1 are shown in Figs. 13–15. The RLS method provides an obvious reduction in vibration magnitude for each of the three controlled modes. The stored electrical energy is observed to increase rapidly at the beginning of the control period; however, in periods of relatively low vibration amplitude, the RLS method loses much of its stored energy in high frequency oscillations. As a result, sustained energy harvesting is not possible.

The SSC method also exhibits a significant reduction in the vibration amplitudes. The SSC method has two major advantages over RLS that improves both its energy harvesting efficiency and vibration suppression performance. One, the SSC method allows

Table 2 Results of the impulse test

	RLS	SSC	MSC	None
Efficiency	0%	10.3%	21.7%	NA
$I_{\text{rms}}(\times 10^{-4}$ m s)	3.02	8.13	1.99	13.5

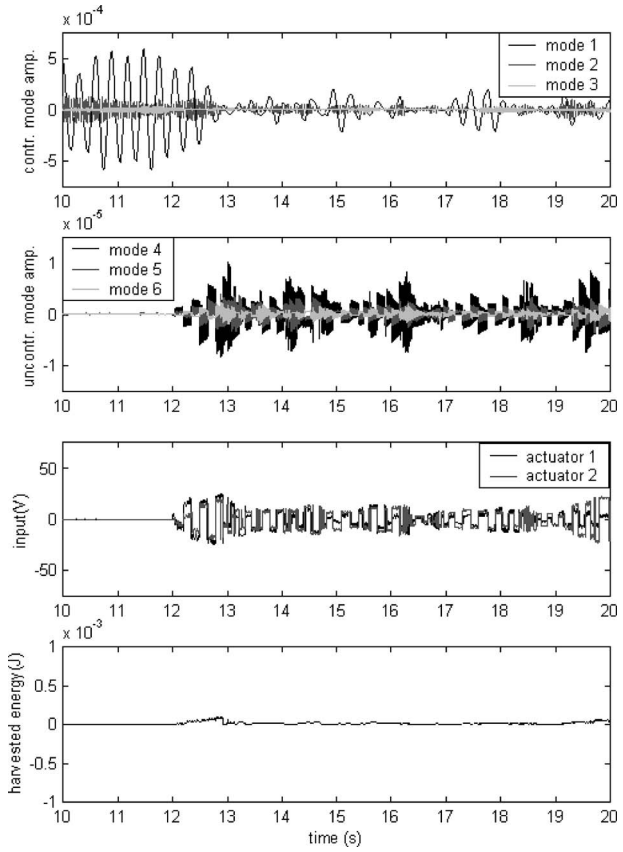

Fig. 13 Random excitation test results for the RLS method (random sequence 1)

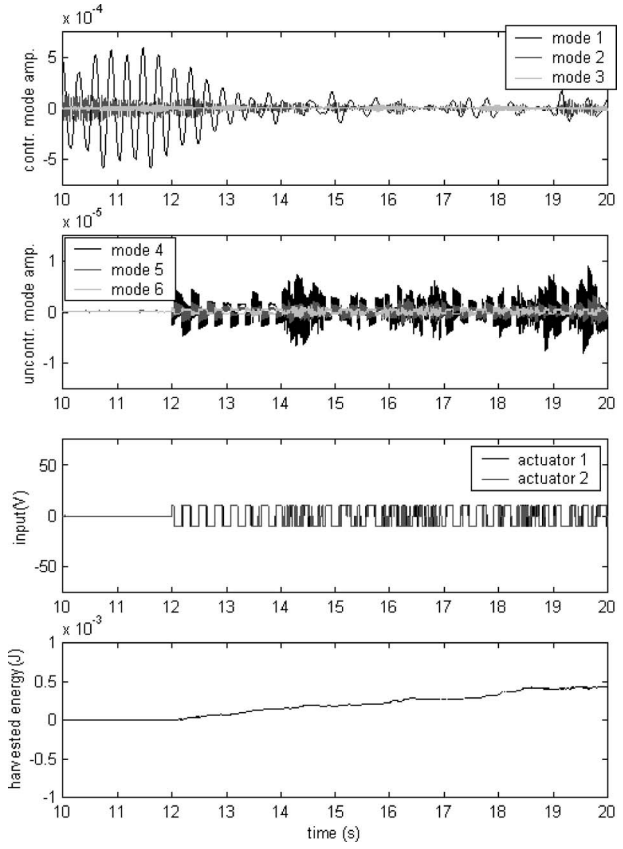

Fig. 14 Random excitation test results for the SSC method (random sequence 1)

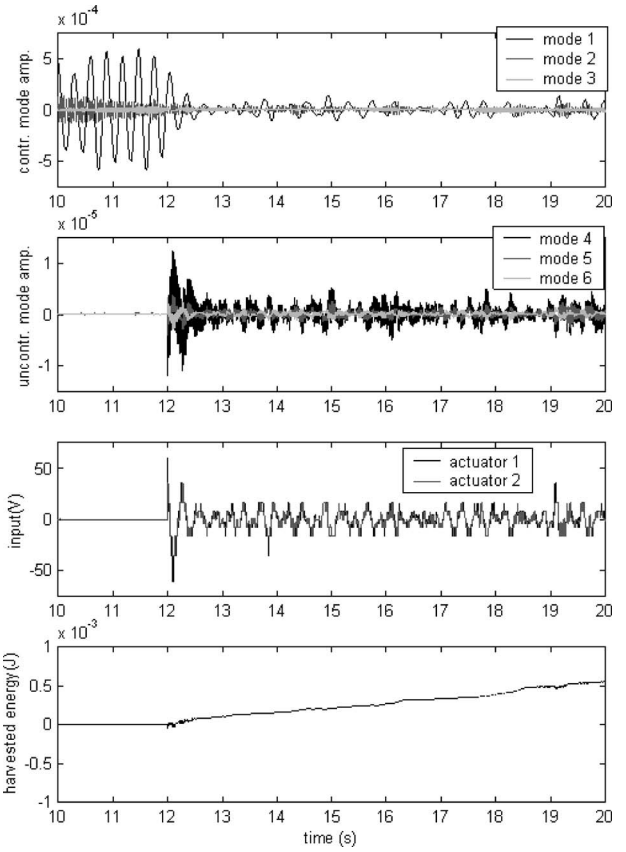

Fig. 15 Random excitation test results for the MSC method (random sequence 1)

an off condition where the stored charge is not subjected to high frequency oscillations at times when no major control effort is needed and energy harvesting opportunity is available. The RLS method requires that the full potential is applied to one side of the actuator or the other at all times as there is no external storage available. Two, the SSC method can reverse the polarity of the control voltages without passing more than a very small amount of the total charge through circuit resistances. In the RLS method, the entirety of accumulated charge must be passed through circuit resistances to change polarity. One such situation occurs at $t = 16.2$ s in Figs. 13–15. At this time the RLS method rapidly reverses its polarity in response to very small but fast vibrations.

While MSC performs only slightly better than SSC in controlling the first three modes, it appears to be significantly more effective in limiting the excitation of the uncontrolled modes. Not only does this provide for smaller overall vibration amplitudes, but it also reduces high frequency oscillations that have a parasitic effect on energy harvesting as the stored charge is rapidly passed back and forth through circuit resistances.

Tables 3 and 4, respectively, contain the energy harvesting efficiencies and vibration suppression metrics for each method and random force sequence. The same data is charted in Figs. 16 and

Table 3 Energy harvesting efficiencies from random excitation tests

Sequence	1	2	3	4	5
RLS	0.25%	0.26%	0.47%	0.54%	1.04%
SSC	19.9%	14.1%	16.1%	18.7%	17.9%
MSC	27.3%	26.2%	23.4%	28.8%	24.1%

Table 4 I_{rms} values from random excitation tests

Sequence	1	2	3	4	5
RLS	8.44×10^{-4}	8.77×10^{-4}	7.01×10^{-4}	7.82×10^{-4}	9.68×10^{-4}
SSC	7.79×10^{-4}	8.61×10^{-4}	5.25×10^{-4}	6.32×10^{-4}	8.29×10^{-4}
MSC	5.41×10^{-4}	5.29×10^{-4}	4.98×10^{-4}	5.00×10^{-4}	5.56×10^{-4}

17.

The results of the random excitation tests largely paralleled the results from the impulse test. As seen in Figs. 16 and 17, the MSC outperformed the other methods in both energy harvesting efficiency and especially vibration suppression for each random sequence. In the case of random excitation, not only did the SSC offer much improved energy harvesting over RLS, but it also provides consistently better vibration suppression.

5 Conclusions

Three different methods of combined vibration reduction and energy harvesting were described and compared in this paper. The RLS method as configured in this investigation cannot continuously harvest and store energy absorbed from mechanical vibrations leading to inferior performance as a self-powering semiactive method. The SSC method affords the capability to suppress vibrations while harvesting and storing energy; however, its single level nature necessitates a lower maximum voltage to facilitate effective energy harvesting, which in turn limits vibration suppression performance. Nonetheless, in some applications, its simplicity over the MSC method may outweigh these limitations. The MSC method was effective in suppressing both transient and continuous random excited vibrations while harvesting over 20% of the mechanical energy in the vibrations. While the MSC method achieved a net positive charge increase over all of the capacitors, the net change in charge was not necessarily positive for each capacitor. Practical implementation of this method would require the energy system mentioned earlier in this paper to redistribute the electrical charge among the capacitors to maintain the nominal voltages in each capacitor. It has been observed that minimizing the excitation of higher frequency uncontrolled modes is a key requirement to facilitate the harvesting of mechanical energy with switched capacitor methods. This highlights the importance of designing the capacitor array based on the particular mechanical system and set of likely disturbances such that large step inputs are minimized. Adaptive algorithms that could adjust the voltage levels on an array of capacitors based on past performance would complement these switched capacitors well.

The results from these simulations suggest that such methods may hold promise in providing a means for effective energy neutral vibration control with applications in many fields. To facilitate practical application, further work is needed to further optimize the energy harvesting, to build in adaptability and robustness to enable the methods to effectively address vibration for which a priori knowledge may be limited, and to optimize state estimation and control algorithms such that they may be implemented with minimal power requirement.

Nomenclature

A = cross-sectional area of the beam or piezoelectric actuator
b_p = electrical-mechanical coupling constant
$\mathbf{B}$ = input matrix
c = Young's modulus of the beam or piezoelectric actuator
C = capacitance
$\mathbf{C}_a$ = constant-length capacitance matrix
D_y = electric displacement in the y-direction
e_y^S = constant-length dielectric constant
E_y = electric field in the y-direction
$f(x,t)$ = external force
$\vec{f}$ = external force vector
h = thickness of the beam or piezoelectric actuator
$H(x)$ = Heaviside function

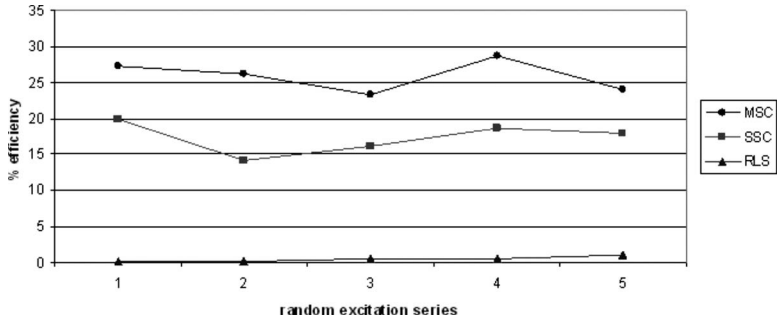

Fig. 16 Energy harvesting efficiencies from random excitation tests

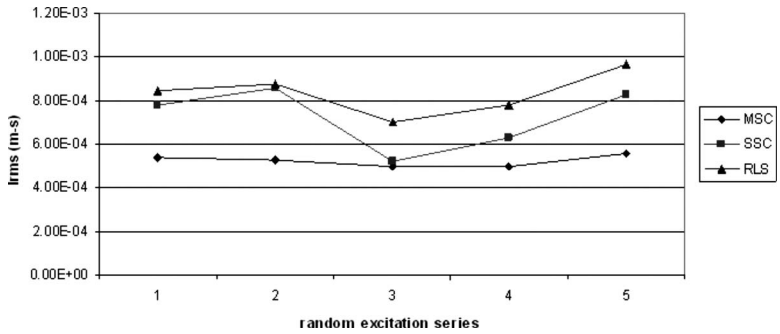

Fig. 17 I_{rms} values from random excitation tests

$i_{p,j}$ = current flowing into the jth piezoelectric actuator
$i_{c,j}$ = current flowing into jth controller
I = geometrical moment of inertia
I_{rms} = performance metric for vibration suppression
J = geometrical moment of the area
L = inductance
L_b = length of the beam
$\vec{p}$ = assumed modal displacement vector
R = circuit resistance
q = electrical charge
Q_j = charge on the jth piezoelectric actuator
$\vec{Q}$ = vector of the piezoelectric actuator charges
T = kinetic energy of the beam or piezoelectric actuator
U = potential energy of the beam or piezoelectric actuator
$\vec{V}_c$ = LQR optimal control voltage vector
$\hat{\vec{V}}_c$ = actual approximation of $\vec{V}_c$
$\hat{V}_{c,j}$ = actual control voltage applied
$V_{p,j}$ = potential across piezoelectric actuator electrodes
$\vec{V}_p$ = vector of $V_{p,j}$
V_t = switching threshold voltage
$V_{\varepsilon,j}$ = strain induced potential in the jth piezoelectric actuator
$w_y(x,t)$ = beam displacement in the y-direction
$\mathbf{W}_1$ = LQR state weighting matrix
$\mathbf{W}_2$ = LQR input weighting matrix
$\mathbf{W}_3$ = LQR state-input cross-product weighting matrix
$x_{1,j}$, $x_{2,j}$ = starting and ending positions of the jth piezoelectric actuator, respectively
x_e = point of action of the external force
$\vec{z}$ = modal state vector
δW = virtual work
δ_{rms} = root mean square of the integrated displacement
ε_x = strain in the x-direction
η = width of the beam or piezoelectric actuator
$\mathbf{\Omega}$ = modal stiffness vector
ρ = mass density of the beam or piezoelectric actuator
σ_x = stress in the x-direction
ς = modal damping coefficient
$\vec{\xi}$ = modal displacement vector
$\mathbf{\Xi}$ = modal damping matrix
ψ_k = kth assumed mode function
Ψ_k = kth mode function

References

[1] Moheimani, S. O. R., and Fleming, A. J., 2006, *Piezoelectric Transducers for Vibration Control and Damping*, Springer, London, p. 271.
[2] Corr, L. R., and Clark, W. W., 2002, "Comparison of Low-Frequency Piezoelectric Switching Shunt Techniques for Structural Damping," Smart Mater. Struct., **11**(3), pp. 370–376.
[3] Makihara, K., Onoda, J., and Tsuchihashi, M., 2006, "Investigation of Performance in Suppressing Various Vibrations With Energy-Recycling Semi-Active Method," Acta Astronaut., **58**(10), pp. 506–514.
[4] Makihara, K., Onoda, J., and Tsuchihashi, M., 2004, "Semi-Active Vibration Suppression of Beam Structures Based on Energy-Recycling Method," Trans. Jpn. Soc. Aeronaut. Space Sci., **47**(157), pp. 167–174.
[5] Corr, L. R., and Clark, W. W., 2003, "A Novel Semi-Active Multi-Modal Vibration Control Law for a Piezoceramic Actuator," Trans. ASME, J. Vib. Acoust., **125**(2), pp. 214–222.
[6] Ottman, G. K., Hoffman, H. F., Bhatt, A. C., and Lesieutre, G. A., 2002, "Adaptive Piezoelectric Energy Harvesting Circuit for Wireless Remote Power Supply," IEEE Trans. Power Electron., **17**(5), pp. 669–676.
[7] Ottman, G. K., Hoffman, H. F., and Lesieutre, G. A., 2003, "Optimized Piezoelectric Energy Harvesting Circuit Using Step Down Converter in Discontinuous Conduction Mode," IEEE Trans. Power Electron., **18**(2), pp. 696–703.
[8] Amritharajah, R., and Chandrakasan, A. P., 1998, "Self-Powered Signal Processing Using Vibration-Based Power Generation," IEEE J. Solid-State Circuits, **33**(5), pp. 687–695.
[9] Lefeuvre, E., Badel, A., Richard, C., and Guyomar, D., 2005, "Piezoelectric Energy Harvesting Device Optimization by Synchronous Electric Charge Optimization," J. Intell. Mater. Syst. Struct., **16**, pp. 865–876.
[10] Ginsberg, J. H., 2001, *Mechanical and Structural Vibrations*, Wiley, New York, p. 692.
[11] Rajamani, R., and Hedrick, J. K., 1991, "Semi-Active Suspensions—A Comparison Between Theory and Experiments," Veh. Syst. Dyn., **20**, pp. 504–518.
[12] Yue, C., Butsuen, T., and Hedrick, J. K., 1988, "Alternative Control Laws for Automotive Suspensions," *Proceedings of the American Control Conference*, Atlanta, GA, June, pp. 2373–2378.